Three-dimensional Ising critical behavior in $R_{0.6}Sr_{0.4}MnO_3$ (R = Pr, Nd) manganites

A. Oleaga and A. Salazar
Departamento de Física Aplicada I, Escuela Técnica Superior de Ingeniería, Universidad del País Vasco/Euskal Herriko Unibertsitatea, Alameda Urquijo s/n, 48013 Bilbao, Spain

M. Ciomaga Hantean and G. Balakrishnan
Department of Physics, University of Warwick, Coventry CV4 7AL, United Kingdom

(Received 21 April 2015; revised manuscript received 25 June 2015; published 13 July 2015)

Magnetic as well as calorimetric measurements have been performed on single crystal samples of $Pr_{0.6}Sr_{0.4}MnO_3$ and $Nd_{0.6}Sr_{0.4}MnO_3$ to develop a complete critical behavior study of the paramagnetic to ferromagnetic transition in both manganites. The critical exponents α,β,γ, and δ have been independently obtained. For $Pr_{0.6}Sr_{0.4}MnO_3$, these are $\alpha = 0.09$, $\beta = 0.312$, $\gamma = 1.106$, and $\delta = 4.545$, while for $Nd_{0.6}Sr_{0.4}MnO_3$ they are $\alpha = 0.11$, $\beta = 0.308$, $\gamma = 1.172$, and $\delta = 4.75$. All these values agree with the three-dimensional (3D)-Ising universality class ($\alpha = 0.11$, $\beta = 0.3265$, $\gamma = 1.237$, and $\delta = 4.79$) and are very far away from any other known universality class. This suggests the presence of magnetocrystalline anisotropies in the system that must be taken into account to fully describe the magnetism of these manganites, which deviates from a simple double exchange model.

DOI: 10.1103/PhysRevB.92.024409 PACS number(s): 64.60.F−, 75.40.Cx, 65.40.−b

I. INTRODUCTION

Scaling analysis within the framework of renormalization group theory assesses that the critical behavior of second order phase transitions in the near vicinity of the critical temperature T_C is characterized by a set of critical exponents associated with different thermal and magnetic properties, whose values are interrelated [1]. Different sets of values of those exponents correspond to different models (universality classes), which have been theoretically developed after a certain expression of the Hamiltonian describing the physical system; the particular values of the exponents have been predicted by different methods [2–5].

The physical magnitudes to which those exponents (named α,β,γ, and δ) are associated are specific heat (c_p), spontaneous magnetization (M_S), inverse of initial susceptibility (χ_0^{-1}), and critical isotherm [$M(H)$ at $T = T_C$], respectively. They fulfill the following equations near T_C, written as a function of the reduced temperature $t = (T - T_C)/T_C$:

$$c_p(T) \sim A^{\pm}|t|^{-\alpha} \quad (A^- \text{ for } T < T_C, \quad A^+ \text{ for } T > T_C), \tag{1}$$

where $A^{\pm}$ are the critical coefficients, whose ratio A^+/A^- is also theorized for each universality class,

$$M_S(T) \sim |t|^{-\beta} \quad (T < T_C), \tag{2}$$

$$\chi_0^{-1}(T) \sim |t|^{\gamma} \quad (T > T_C), \tag{3}$$

$$M(H) \sim H^{1/\delta} \quad (T = T_C). \tag{4}$$

Finally, the magnetic equation of state in the critical region is given by

$$M(H,t) = |t|^{\beta} f_{\pm}\left(H/|t|^{\beta+\gamma}\right), \tag{5}$$

where f_- and f_+ are regular analytic functions for $T < T_C$ and $T > T_C$, respectively.

The following scaling laws give the relations among the critical exponents

$$\alpha + 2\beta + \gamma = 2 \tag{6}$$

$$\delta = 1 + \gamma/\beta. \tag{7}$$

The attribution of a certain second order phase transition to a particular class gives an insight of the underlying physics, such as the range and dimensionality of the magnetic exchange interactions as well as the role that other mechanisms can play if the critical parameters obtained do not exactly comply with one of those classes (role of spin-orbit interactions or dipolar long-range order interactions, for instance). Table I summarizes the values of the critical exponents and coefficients for the most common universality classes of application in the case of ferromagnetic materials when dimensionality is three. The mean field model is equivalent to the classical Landau model and is based on long-range interactions. The other three models describe the ferromagnetic phenomena on the basis of short range interactions among the spins: the Heisenberg model corresponds to an isotropic ferromagnetic material, the XY model is of application when there is an easy plane for the magnetization, and the Ising model is applicable when there is a uniaxial anisotropy. It is worth analyzing the difference among the particular values that the critical exponents take in the different models. The ones obtained from magnetic measurements (β and γ) increase their values from the uniaxial anisotropic model (Ising) to the isotropic one (Heisenberg), but the difference is small, which sometimes makes it difficult to discriminate among the models. On the other hand, the critical exponent associated with the specific heat α changes its sign from one model to the other one, and the ratio of the critical parameters A^+/A^- is very different (from 0.53 to 1.52). So, even if Eq. (6) tells us that it would be enough with the magnetic critical exponents to elucidate the universality class to which the phase transition belongs (without the need to evaluate α), it is safer to independently obtain all three parameters to extract

TABLE I. Main universality classes for magnetic systems (Refs. [2–5]).

Universality class	α	β	γ	δ	A^+/A^-
Mean-field Model	0	0.5	1.0	3.0	-
3D-Ising	0.11	0.3265	1.237	4.79	0.53
3D-XY	− 0.014	0.34	1.30	4.82	1.06
3D-Heisenberg	− 0.115	0.365	1.386	4.80	1.52

sensible conclusions. Finally, δ is not useful to discriminate among the short-range models as its value is nearly the same in the three of them, but it is important to extract it independently from experiments as a further confirmation.

Another important issue when studying critical behavior is to do it on appropriate samples. It is well known that single crystals are ideal for that kind of study as polycrystalline samples present a strong smearing in the phase transitions, making it difficult to evaluate the critical parameters. Besides, in order to fully reveal the critical behavior, high quality crystals are needed, with good stoichiometry and as few defects as possible, as the real critical behavior might be masked if this is not achieved.

In this paper, the critical behavior study of two ferromagnetic phase transitions in manganites is carried out in $Pr_{0.6}Sr_{0.4}MnO_3$ and $Nd_{0.6}Sr_{0.4}MnO_3$. We have selected this particular concentration (substituting 40% the rare-earth ion with Sr) as it is the one at which the colossal magnetoresistance (CMR) is especially important and for which the low temperature phase is ferromagnetic in the whole temperature range [6,7]. It can be seen from the phase diagrams that both $Pr_{1-x}Sr_xMnO_3$ and $Nd_{1-x}Sr_xMnO_3$ are very similar in the region around $x = 0.4$ (paramagnetic insulator above T_C, ferromagnetic metallic under it, with close values of T_C) so the study of the critical behavior of both of them using the same techniques and under the same conditions could give valuable information about the appropriateness of a physical description simply by means of a double exchange interaction, which would be described by a Heisenberg model [8] or if any other mechanisms must be taken into account, such as magnetic anisotropies, disorder, dipolar interactions, phase separation, and such.

There are many studies on the critical behavior of different manganites, but there is a lack of systematic research on its evolution as doping is introduced in a particular parent compound. The starting point is similar in both cases as $PrMnO_3$ and $NdMnO_3$ have been found to belong to the three-dimensional (3D)-Heisenberg case, though not as perfectly as in the case of $LaMnO_3$ [9]; however, all three parent compounds are antiferromagnets while they turn into metallic ferromagnets when they are hole-doped. The way this affects their critical behavior is far from being well established. Several studies have been already made on the critical behavior of $R_{1-x}Sr_xMnO_3 (R = La, Pr, Nd)$ for Sr concentrations in the ferromagnetic metallic region (which corresponds to $0.25 \leqslant x \leqslant 0.45$ for Pr and Nd and in the case of La to x higher than ≈ 0.18), but the conclusions differ and, in some cases, are not well substantiated.

In the case of $La_{1-x}Sr_xMnO_3$ (the most studied one by far), some authors claim that long-range interactions describe well that transition by means of a mean field model (see Mohan *et al.* and Schwartz *et al.* for $x = 0.2$ [10,11], Lofland *et al.* for $x = 0.3$) [12], Nair *et al.* found for $x = 0.125$ critical exponents with values corresponding to the Heisenberg model [13], Ghosh *et al.* found Heisenberg exponents for $x = 0.3$ [14], while the values obtained by Vasiliu-Doloc and Lynn ($x = 0.2, 0.3$) [15], Martin *et al.*($x = 0.3$) [16], Kim *et al.* ($x = 0.25$) [17], Oleaga *et al.*($x = 0.30$) [18], and Lin *et al.*($x = 0.3$) [19] all sustain the anisotropic Ising model.

The critical behavior of $Pr_{1-x}Sr_xMnO_3$ has not been studied much in this region. The particular concentration $x = 0.4$ has been studied by Hcini *et al.* [20], Rößler *et al.* [21], and Masheswar Repaka *et al.* [22]. They all claim that the suitable model is the Heisenberg model, but even if the β exponent they found is around the theoretical one, γ is between Heisenberg and Ising. There is another paper on $x = 0.45$ by Fan *et al.* where their conclusion is that a mean field model is of application [23].

Finally, $Nd_{1-x}Sr_xMnO_3$ has been scarcely studied in the ferromagnetic metallic region. A paper on $x = 0.3$ by Venkatesh *et al.* gave critical exponents between the mean field model and the Heisenberg one [24]; Oleaga *et al.*, measuring thermal diffusivity, concluded that the Ising model better illustrated the transition for $x = 0.4$ [25].

One of the drawbacks of several of the studies performed is that they have been done on polycrystalline samples, where it is much more difficult to extract information about the critical behavior of the transition. In most of the papers cited above, only the magnetic exponents have been extracted, without employing techniques that can also bring the critical exponent α and the critical ratio A^+/A^-.

Thus, the aim of this paper is to make a complete study of the critical behavior of $Pr_{0.6}Sr_{0.4}MnO_3$ and $Nd_{0.6}Sr_{0.4}MnO_3$ on high quality single crystals, grown at the same lab, applying high resolution calorimetric techniques as well as magnetic ones to extract independently all critical parameters α, A^+/A^-, β, γ, and δ and trying to elucidate which universality class best suits the results.

II. SAMPLES AND EXPERIMENTAL TECHNIQUES

Single crystals $Pr_{0.6}Sr_{0.4}MnO_3$ and $Nd_{0.6}Sr_{0.4}MnO_3$ were grown by the floating zone technique using a two mirror optical furnace, in air, using growth speeds of around 4–6 mm/h [26]. Crystal quality and orientation were determined using the x-ray Laue diffraction technique. The crystals were cut from the as-grown boule in the shape of plane-parallel slabs of around 500 μm thickness for the measurements.

Magnetization (M) measurements have been carried out in a vibrating sample magnetometer (VSM) by Cryogenic Limited under external applied magnetic fields H_a ranging from 0 to 80 kOe. Isotherms were collected over a range of about ±15 K around T_C ($\Delta T = 1$ K) in order to adequately cover the critical region. The magnetic field H_a has been corrected for demagnetization effects to extract the internal field using the relation $H_i = H_a - NM$, where M is the measured magnetization and N is the demagnetization factor. N has been obtained from ac susceptibility measurements following the method given by Jiang *et al.* [27], and the obtained H_i has been used for the scaling analysis. The

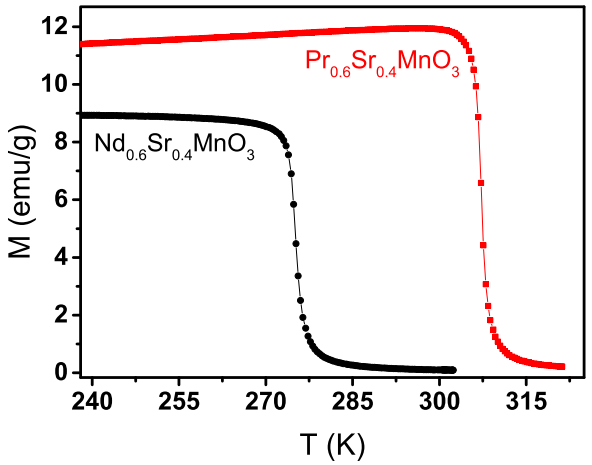

FIG. 1. (Color online) Magnetization as a function of temperature measured in a field-cooled state using a magnetic field of 100 Oe for $Pr_{0.6}Sr_{0.4}MnO_3$ (■) and $Nd_{0.6}Sr_{0.4}MnO_3$ (●).

magnetic susceptibility was measured with AC Measurement System Option in Physical Properties Measurement System (PPMS) by Quantum Design. The demagnetization factors obtained have been $N = 9.3$ gOe/emu for $Pr_{0.6}Sr_{0.4}MnO_3$ and $N = 14.0$ gOe/emu for $Nd_{0.6}Sr_{0.4}MnO_3$.

The specific heat measurements have been carried out with a high resolution ac photopyroelectric calorimeter in the back detection configuration. The details of the experimental setup, as well as of the theory that explains how the thermal parameters are obtained from the photopyroelectric signal can be found elsewhere [28–30]. The range of cooling and heating rates used has been from 60 mK/min for measurements on a wide temperature range down to 10 mK/min for high-resolution runs close to T_C covering a similar range as in the case of the magnetic measurements.

III. EXPERIMENTAL RESULTS AND FITTINGS

Figure 1 shows the magnetization of both samples as a function of temperature under an applied field of 100 Oe where the very well known ferromagnetic transitions are displayed. The transition temperatures obtained from these measurements are $T_C \approx 307.5$ K for $Pr_{0.6}Sr_{0.4}MnO_3$ and $T_C \approx 276$ K for $Nd_{0.6}Sr_{0.4}MnO_3$. In what follows, the full scaling analysis will be presented for each sample, presenting first the magnetic measurements and then the specific heat ones in each case.

A. $Pr_{0.6}Sr_{0.4}MnO_3$

Figure 2(a) contains the standard Arrott Plot, where M^2 is represented as a function of H/M (in what follows, H will always be the internal field H_i) for isotherms in the temperature range 292–322 K. If long-range interactions were responsible for the ferromagnetic transition, there would be a linear behavior at high fields, which clearly is not the case. As all curves present a downward slope, a nonmean field behavior is present in this case. Following the Banerjee

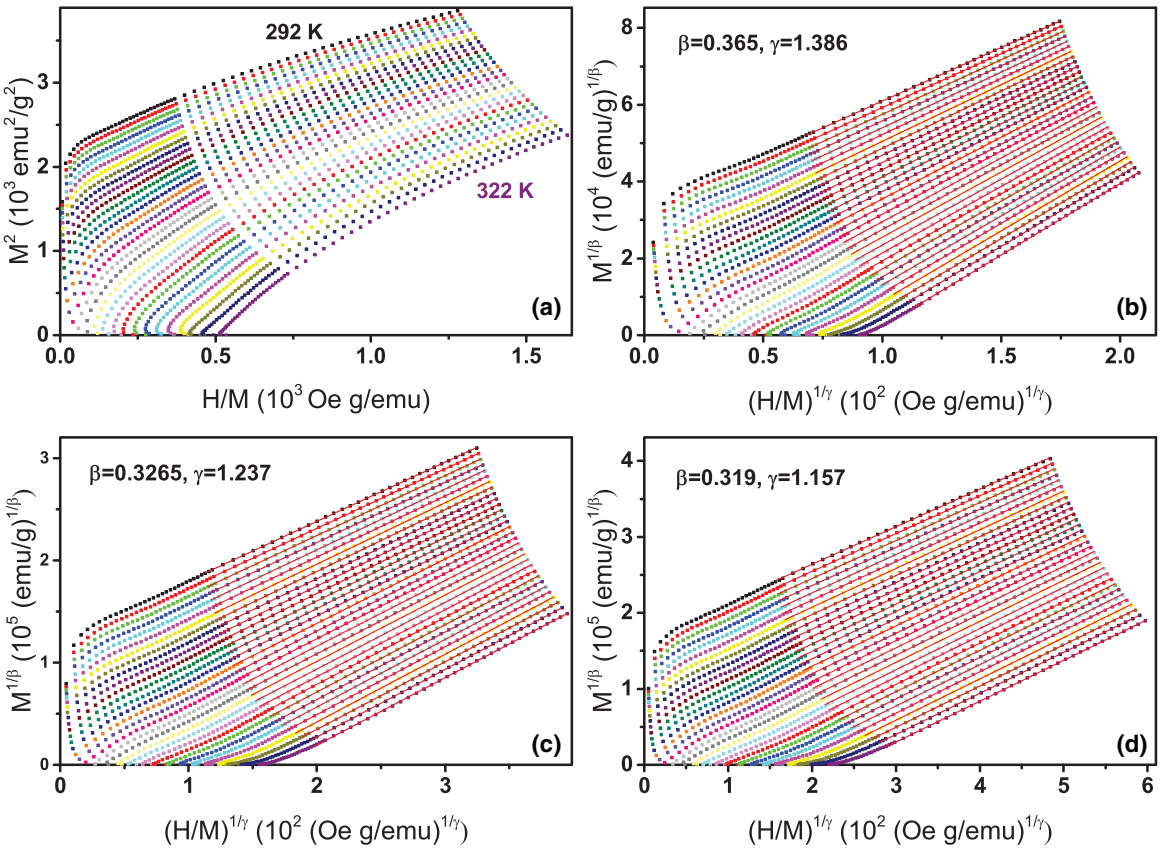

FIG. 2. (Color online) (a) Arrott Plot of isotherms collected around T_C for $Pr_{0.6}Sr_{0.4}MnO_3$. MAPs with the Heisenberg (b) and Ising (c) trial exponents showing the parallelism of the linear fittings at high fields. (d) Optimized MAP after the iteration procedure.

criterion [31], the positive slope of the curves confirms the second order character of the transition. To establish the value of the critical exponents and thus the class of universality to which $Pr_{0.6}Sr_{0.4}MnO_3$ might belong, we have turned our attention to the Modified Arrott Plots (MAPs), plotting $M^{1/\beta}$ versus $(H/M)^{1/\gamma}$. As starting trial values, we have taken the ones corresponding to the Heisenberg ($\beta = 0.365$, $\gamma = 1.386$) and Ising models ($\beta = 0.3265$, $\gamma = 1.2372$), which are shown in Figs. 2(b) and 2(c), respectively. Linear fittings of the experimental points in those graphs at high field values do not render perfect parallel curves but are much better in the case of the Ising class than in the Heisenberg one. This can be visually seen but also quantitatively evaluated by the deviation of the slopes with respect to the average value, which is $\pm 15\%$ for Heisenberg exponents and $\pm 8\%$ for the Ising case. So the Ising exponents have been taken as the starting point from which a rigorous iterative process has been carried out. A linear extrapolation of the isotherms in Fig. 2(c) has been taken from the high field values to extract $(M_S)^{1/\beta}$ and $(\chi_0^{-1})^{1/\gamma}$ as an intercept on $M^{1/\beta}$ and $(H/M)^{1/\gamma}$ axis, respectively. These values of $M_S(T)$ and $\chi_0^{-1}(T)$ have been independently fitted to Eqs. (2) and (3), respectively, thus extracting new values of β and γ. The process is repeated till convergence is reached and the best values of β, γ, and T_C, which give the best parallelism, are obtained, which in this case are $\beta = 0.319 \pm 0.01$ and $\gamma = 1.157 \pm 0.007$ [the MAP corresponding to these values is shown in Fig. 2(d)]. The obtained $M_S(T)$ and $\chi_0^{-1}(T)$ are plotted as a function of temperature in Fig. 3, whose fit to Eq. (2) gives $\beta = 0.3147 \pm 0.006$, $T_C = 308.27 \pm 0.01$ K and to Eq. (3) gives $\gamma = 1.095 \pm 0.07$, $T_C = 308.37 \pm 0.04$ K. Both values are very close to the Ising theoretical values (see Table I).

As the next step in the scaling analysis, we have followed the Kouvel Fisher method to determine more accurately β,γ, and T_C [32]. After this method, both $M_S(dM_S/dT)^{-1}$ and $\chi_0^{-1}(d\chi_0^{-1}/dT)^{-1}$ have a linear behavior with respect to T, with slopes $1/\beta$ and $1/\gamma$, respectively. One of the advantages of this method is that the value of the critical temperature is not introduced *a priori* but extracted from the intercept of the straight fitted lines on the temperature axis. The Kouvel Fisher plot is shown in Fig. 4. The critical parameters obtained are $\beta = 0.312 \pm 0.002$, $T_C = 308.20 \pm 0.02$ K, $\gamma = 1.106 \pm 0.005$, and $T_C = 308.32 \pm 0.04$ K. It is worth remarking how MAPs and the Kouvel Fisher method give close values of all critical parameters, confirming the robustness of the results.

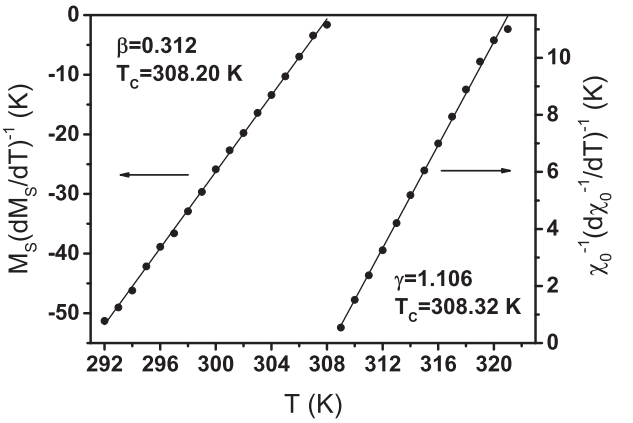

FIG. 4. Kouvel Fisher plot of spontaneous magnetization (left) and inverse of initial susceptibility (right) for $Pr_{0.6}Sr_{0.4}MnO_3$. The straight lines are linear fits, from which T_C and the critical exponents are obtained.

After Eq. (4), the critical exponent δ can be extracted from the fitting of the critical isotherm to be compared with the values obtained from the scaling law [Eq. (7)]. Figure 5 shows the critical isotherm at $T = 308$ K in log-log scale as this should render a straight line (as it happens), whose slope is δ. In this particular case, the fitting gives $\delta = 4.545 \pm 0.008$, while the values extracted using Eq. (7) from MAP is 4.48 ± 0.03 and Kouvel-Fisher method 4.54 ± 0.04. So there is a strong coherence among the different results. All the exponents obtained are listed in Table II.

The last confirmation of the validity of the results obtained so far would come from the equation of state Eq. (5) if it were fulfilled with the obtained critical exponents. Figure 6 shows how all results collapse into two different branches, below and

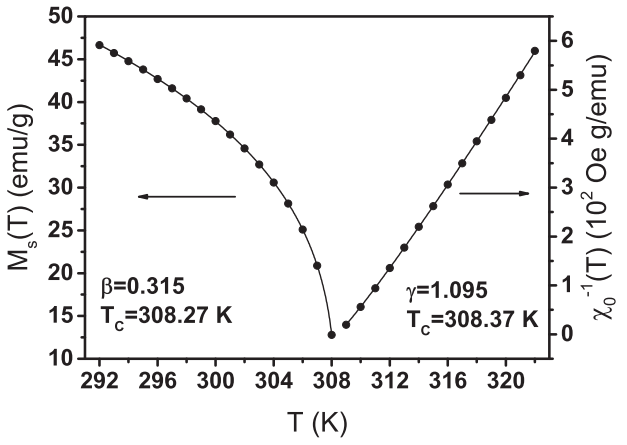

FIG. 3. Spontaneous magnetization (left) and inverse of initial susceptibility (right) vs temperature for $Pr_{0.6}Sr_{0.4}MnO_3$ as obtained from the optimized MAP. The solid curves correspond to the fits to Eqs. (2) and (3), as explained in the text.

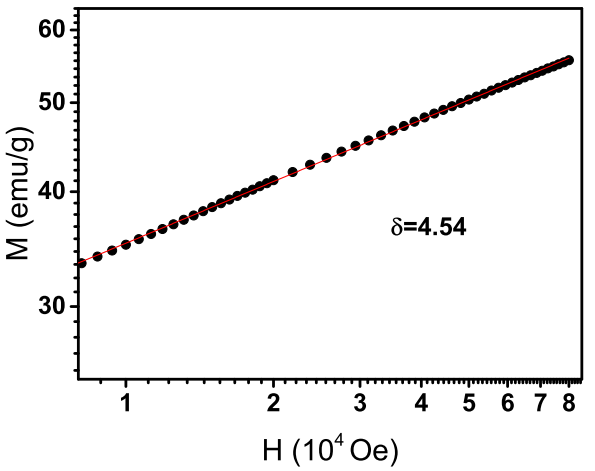

FIG. 5. (Color online) M vs H plot in a log-log scale collected at $T = 308$ K ($\approx T_C$) for $Pr_{0.6}Sr_{0.4}MnO_3$. The straight line is the linear fit from which the exponent δ is obtained.

TABLE II. Values of the obtained critical exponents and parameters β, γ, δ, α, and A^+/A^-.

Material	Technique	β	γ	δ	α	A^+/A^-
$Pr_{0.6}Sr_{0.4}MnO_3$	Modified Arrott Plot	0.3147 ± 0.0006	1.095 ± 0.007	4.48 ± 0.03[a]		
	Kouvel-Fisher Method	0.312 ± 0.002	1.106 ± 0.005	4.54 ± 0.04[a]		
	Critical Isotherm			4.545 ± 0.008		
	Photopyroelectric calorimetry				0.09 ± 0.01	0.57 ± 0.15
$Nd_{0.6}Sr_{0.4}MnO_3$	Modified Arrott Plot	0.321 ± 0.003	1.183 ± 0.017	4.68 ± 0.08[a]		
	Kouvel-Fisher Method	0.308 ± 0.004	1.172 ± 0.011	4.80 ± 0.09[a]		
	Critical Isotherm			4.75 ± 0.02		
	Photopyroelectric calorimetry				0.11 ± 0.02	0.52 ± 0.19

[a]Calculated from Eq. (7) $\delta = 1 + \gamma/\beta$.

above T_C. This is generally taken as the most severe test for proper scaling.

The value of the critical exponent α can be evaluated from Eq. (6), but in order to confirm the universality class to which $Pr_{0.6}Sr_{0.4}MnO_3$ belongs, it is especially interesting to obtain it independently from calorimetric experiments. As explained in Sec. II, an ac photopyroelectric calorimeter has been used to obtain high resolution specific heat data in the near vicinity of T_C. See the revision paper by Zammit *et al.* [33], where a full description of the capabilities of this technique to study critical behavior of second order phase transitions is presented.

The experimental specific heat curves have been fitted to the well-known equation:

$$c_p = B + Ct + A^{\pm}|t|^{-\alpha}(1 + E^{\pm}|t|^{0.5}), \qquad (8)$$

where $t = (T - T_C)/T_C$ is the reduced temperature and α, $A^{\pm}$, B, C, and $E^{\pm}$ are adjustable parameters. Superscripts $+$ and $-$ stand for $t > T_C$ and $t < T_C$, respectively. The linear term represents the background contribution to the specific heat, while the last term is the anomalous contribution to the specific heat. The factor under parenthesis is the correction to scaling that represents a singular contribution to the leading power, as known from experiments and theory. A nonlinear least square routine using a Levenberg-Marquardt method has been used to simultaneously fit the experimental data for $t > T_C$ and $t < T_C$. The details of the fitting procedure can be found elsewhere [34].

Figure 7 shows the experimental specific heat curve in the near vicinity of the critical temperature as well as the fitting, along with the deviation plot of the fitting with respect to the

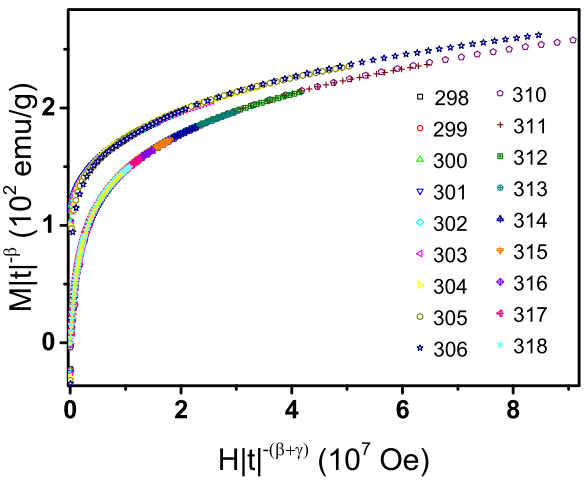

FIG. 6. (Color online) The renormalized magnetization plotted as a function of the renormalized field following Eq. (5) for $Pr_{0.6}Sr_{0.4}MnO_3$. All data collapse in two separate branches, one above and one below T_C.

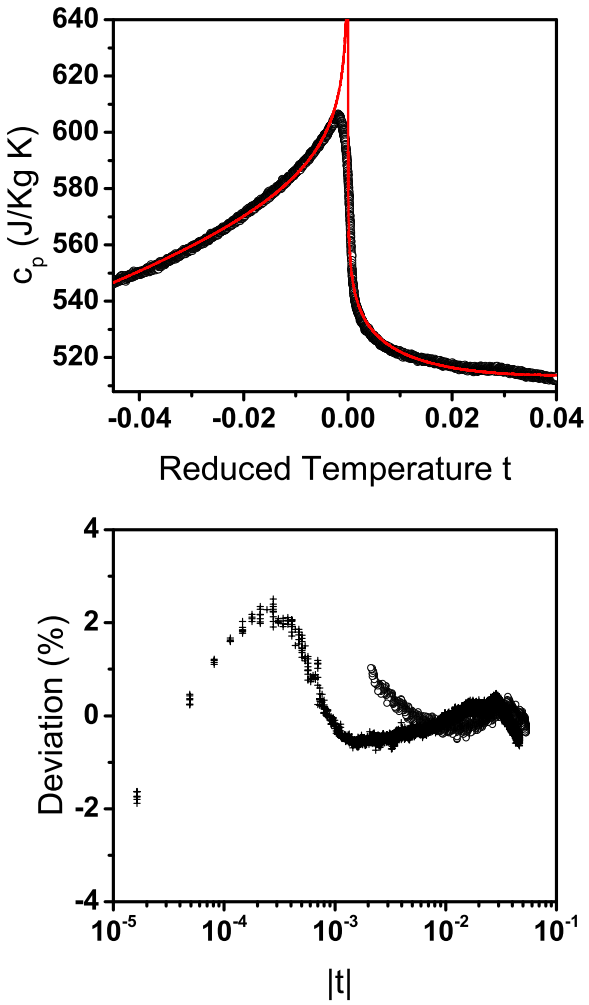

FIG. 7. (Color online) Experimental (dots) and fitted curves (continuous lines) of the specific heat as a function of the reduced temperature for $Pr_{0.6}Sr_{0.4}MnO_3$ in the near vicinity of T_C (top). And the deviation plots for the fittings (bottom). Open circles are for $T < T_C$, crosses are for $T > T_C$.

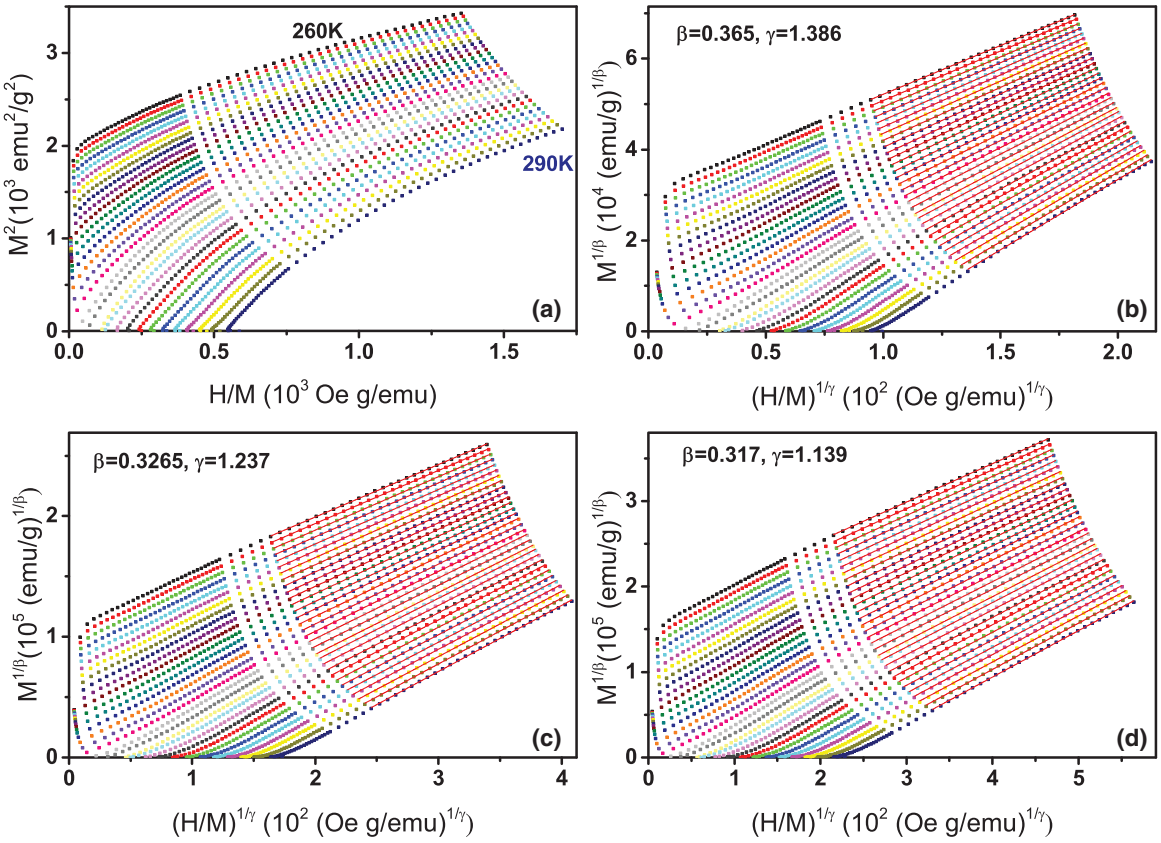

FIG. 8. (Color online) (a) Arrott Plots of isotherms collected around T_C for $Nd_{0.6}Sr_{0.4}MnO_3$. MAPs with the Heisenberg (b) and Ising (c) trial exponents showing the parallelism of the linear fittings at high fields. (d) Optimized MAPs after the iteration procedure.

experimental curve. The fitting is quite good, and the obtained parameters are $\alpha = 0.09 \pm 0.01$, $A^+/A^- = 0.57 \pm 0.15$ (for the Ising class these are $\alpha = 0.11$, $A^+/A^- = 0.53$), having used a fitting range of $5.3 \times 10^{-2} - 4 \times 10^{-3}$ for $t < T_C$ and $4.6 \times 10^{-2} - 1.6 \times 10^{-5}$ for $t > T_C$. One of the advantages of this technique is that we can get really close to the critical temperature. As a confirmation test, a fitting was intended using the theoretical Heisenberg exponents and parameters, but no fitting was found, the exponents kept turning to the Ising ones. The final values have been included in Table II.

This means that all critical exponents and parameters α, $A^{\pm}$, β, γ, and δ agree with the anisotropic Ising model.

B. $Nd_{0.6}Sr_{0.4}MnO_3$

An equivalent analysis to the one performed on $Pr_{0.6}Sr_{0.4}MnO_3$ has been carried out with $Nd_{0.6}Sr_{0.4}MnO_3$. Figure 8(a) contains the standard Arrott Plot for isotherms in the temperature range 260–290 K. Again, a mean field model does not describe well the critical behavior of this transition, which is confirmed as second order by the positive slope of the curves. Figures 8(b) and 8(c) show the MAPs, with the Heisenberg and Ising exponents as trial values. Once again, the linear fittings of the experimental points at high field values give a better parallelism for the Ising class than for the Heisenberg one. The deviation of the slopes with respect to the average value is ±19% for Heisenberg exponents and ±12% for the Ising case. Thus, the same rigorous iterative process has been carried out starting with the Ising values. The values for which the best parallelism is found are $\beta = 0.317 \pm 0.006$ and $\gamma = 1.139 \pm 0.010$, and this is shown in Fig. 8(d). The values of $M_S(T)$ and $\chi_0^{-1}(T)$ obtained from that graph are plotted as a function of temperature in Fig. 9, whose fit to Eq. (2) gives $\beta = 0.321 \pm 0.003$ and $T_C = 277.17 \pm 0.03$ K, and to Eq. (3) gives $\gamma = 1.183 \pm 0.017$ and $T_C = 277.21 \pm 0.09$ K. Both values are quite close to the Ising theoretical values.

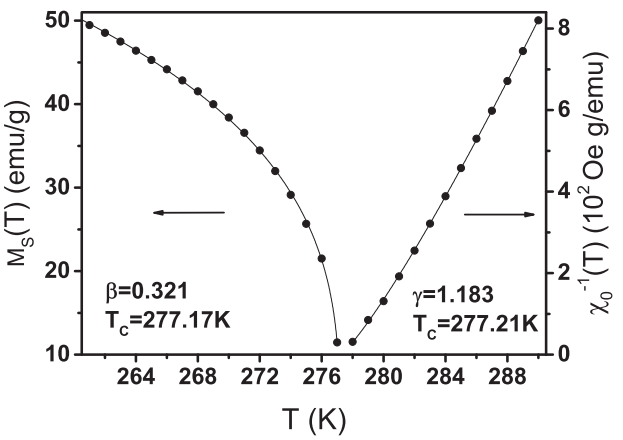

FIG. 9. Spontaneous magnetization (left) and initial susceptibility (right) vs temperature for $Nd_{0.6}Sr_{0.4}MnO_3$ as obtained from the optimized MAP. The solid curves correspond to the fits to Eqs. (2) and (3), as explained in the text.

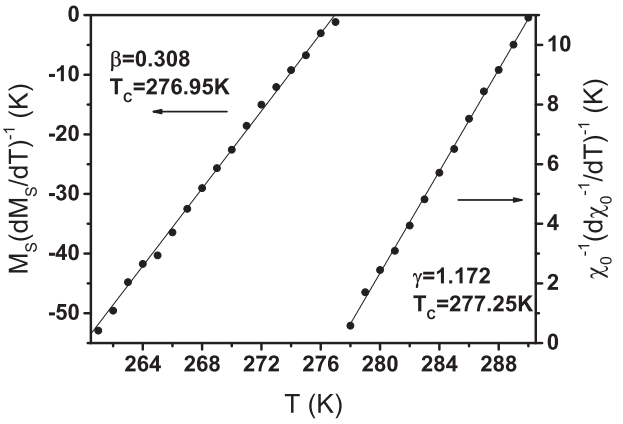

FIG. 10. Kouvel Fisher plot of spontaneous magnetization (left) and inverse of initial susceptibility (right) for $Nd_{0.6}Sr_{0.4}MnO_3$. The straight lines are linear fits, from which T_C and the critical exponents are obtained.

Figure 10 shows the Kouvel Fisher plots, from whose fittings the critical parameters $\beta = 0.308 \pm 0.004$, $T_C = 276.95 \pm 0.06$ K, $\gamma = 1.172 \pm 0.011$, and $T_C = 277.25 \pm 0.07$ K are obtained. It is worth remarking how MAPs and the Kouvel Fisher method again give close values of all critical parameters, confirming the robustness of the results.

Figure 11 shows the critical isotherm at $T = 277$ K in log-log scale, which gives a straight line of slope δ. In this particular case, the fitting gives $\delta = 4.75 \pm 0.02$ while the values extracted using Eq. (7) from MAP is 4.68 ± 0.08 and the Kouvel-Fisher method is 4.80 ± 0.09. So there is a strong coherence among the different results. All the critical exponents found are listed in Table II.

Figure 12 shows the plot corresponding to the equation of state Eq. (5) with those critical exponents found. All results collapse into two different branches, below and above T_C, though not as well as in the case of $Pr_{0.6}Sr_{0.4}MnO_3$.

Finally, critical exponent α has been obtained by measuring and fitting the specific heat, and this is shown in Fig. 13. The fitting agrees quite well with the experimental results,

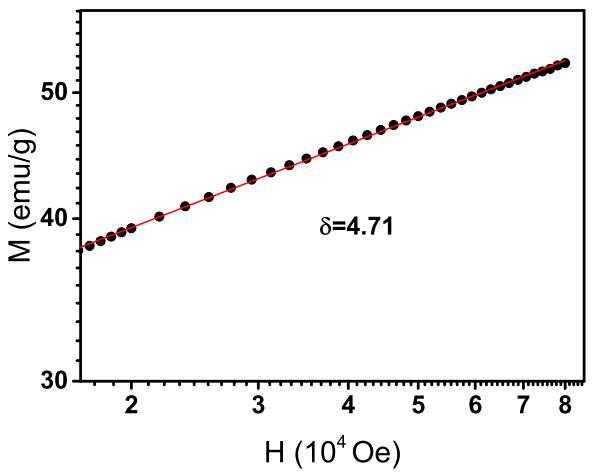

FIG. 11. (Color online) M vs H plot in a log-log scale collected at $T = 277$ K ($\approx T_C$) for $Nd_{0.6}Sr_{0.4}MnO_3$. The straight line is the linear fit from which the exponent δ is obtained.

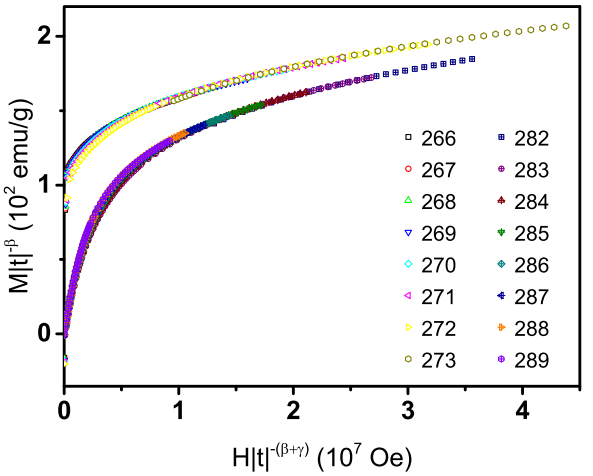

FIG. 12. (Color online) The renormalized magnetization plotted as a function of the renormalized field following Eq. (5) for $Nd_{0.6}Sr_{0.4}MnO_3$. All data collapse in two separate branches, one above and one below T_C.

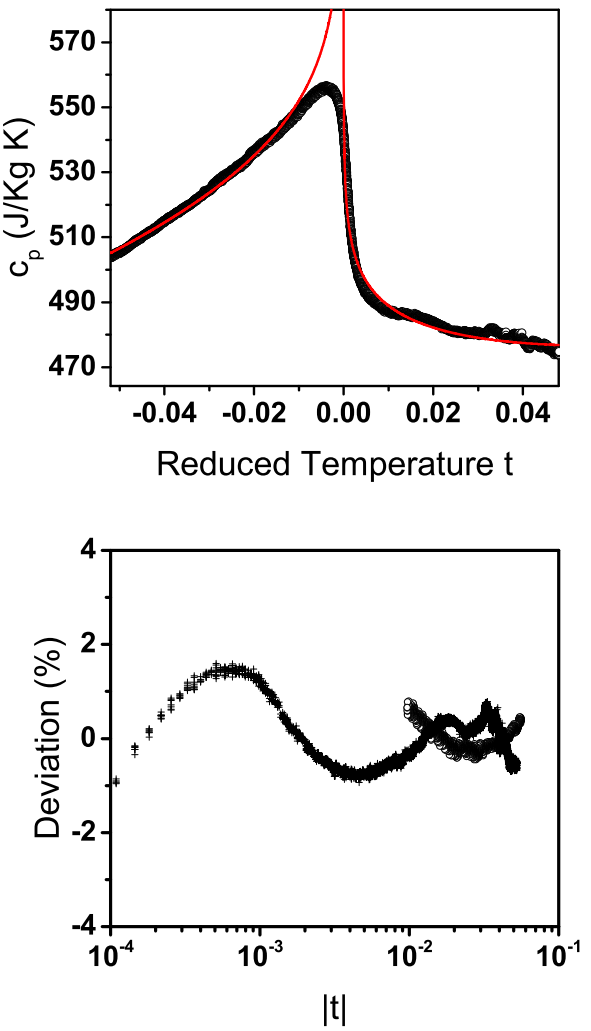

FIG. 13. (Color online) Experimental (dots) and fitted curves (continuous lines) of the specific heat as a function of the reduced temperature for $Nd_{0.6}Sr_{0.4}MnO_3$ in the near vicinity of T_C (top). And the deviation plots for the fittings (bottom). Open circles are for $T < T_C$, crosses for $T > T_C$.

TABLE III. Critical exponents α,β,γ in literature and in this work.

Material	Author	α	β	γ
$PrMnO_3$	Oleaga *et al.* [9]	−0.11		
$Pr_{0.6}Sr_{0.4}MnO_3$	Hcni *et al.* [20]		0.379	1.304
	Röβler *et al.* [21]	−0.13	0.365	1.309
	Masheswar Repaka *et al.* [22]		0.364	1.336
	This work	+0.09	0.312	1.106
$Pr_{0.55}Sr_{0.45}MnO_3$	Fan *et al.* [23]		0.462	1.033
$Pr_{0.52}Sr_{0.48}MnO_3$	Sabayasachi *et al.* [47]		0.462	1.210
$Pr_{0.5}Sr_{0.5}MnO_3$	Pramanik *et al.* [46]		0.448	1.334
$NdMnO_3$	Oleaga *et al.* [9]	−0.11		
$Nd_{0.7}Sr_{0.3}MnO_3$	Ventakesh *et al.* [24]		0.57	1.16
$Nd_{0.6}Sr_{0.4}MnO_3$	Oleaga *et al.* [25]	+0.12		
	This work	+0.11	0.308	1.172
$LaMnO_3$	Oleaga *et al.* [9]	−0.10		
$La_{0.875}Sr_{0.125}MnO_3$	Nair *et al.* [13]		0.37	1.38
$La_{0.8}Sr_{0.2}MnO_3$	Mohan *et al.* [10]		0.5	1.05
	Schwartz *et al.* [11]		0.45	
	Vasiliu-Doloc *et al.* [15]		0.30	
$La_{0.75}Sr_{0.25}MnO_3$	Kim *et al.* [17]	+0.05	0.40	1.27
$La_{0.7}Sr_{0.3}MnO_3$	Lofland *et al.* [12]		0.45	
	Gosh *et al.* [14]		0.37	1.22
	Vasiliu-Doloc *et al.* [15]		0.30	
	Martin *et al.* [16]		0.295	
	Oleaga *et al.* [18]	+0.11		
	Lin *et al.* [19]		0.31	
$La_{0.65}Sr_{0.35}MnO_3$	Oleaga *et al.* [18]	+0.11		
$La_{0.8}Ca_{0.2}MnO_3$	Zhang *et al.* [42]		0.259–0.349	0.918–1.231
	Jiang *et al.* [43]		0.37	1.38
	Ferreira *et al.* [44]	≈+0.2		
$La_{0.75}Ca_{0.25}MnO_3$	Jiang *et al.* [43]		0.12	1.62
$La_{0.6}Ca_{0.4}MnO_3$	Kim *et al.* [41]	+0.48	0.25	1.03
	Zhang *et al.* [42]		0.2549–0.263	0.776–1.008
	Ferreira *et al.* [44]	≈+0.18		
$Pr_{0.75}Ca_{0.25}MnO_3$	Ho *et al.* [45]		0.351	1.372
$Pr_{0.73}Ca_{0.27}MnO_3$	Ho *et al.* [45]		0.362	1.132
	Jiang *et al.* [27]		0.36	1.36
$Pr_{0.71}Ca_{0.29}MnO_3$	Ho *et al.* [45]		0.521	0.912
	Jiang *et al.* [27]		0.37	1.38

though not as nicely as in the previous sample; the obtained parameters are $\alpha = 0.10 \pm 0.02$, $A^+/A^- = 0.52$, having used a fitting range of $4.8 \times 10^{-2} - 9.4 \times 10^{-3}$ for $t < T_C$ and $4.6 \times 10^{-2} - 1.1 \times 10^{-4}$ for $t > T_C$. It was also confirmed that the theoretical Heisenberg parameters did not allow the fitting of the curve.

Thus, also in this second case, all critical exponents $\alpha, A^{\pm}, \beta, \gamma$, and δ agree with the anisotropic Ising model.

IV. DISCUSSION

All the experimental results and fittings shown in the previous section are clearly in agreement with the 3D-Ising universality class, thus stating that the effects of magnetocrystalline anisotropies are the leading terms in the critical fluctuations close to the critical temperature, in opposition to the exchange mechanism, which is consistent with the 3D-Heisenberg class. A crossover behavior from a long-range mean field model to a short range one is expected as T_C is approached due to the growing relevance of the critical fluctuations of the order parameter. Kim *et al.* found in a similar system ($La_{0.75}Sr_{0.25}MnO_3$) [17] that the expected crossover sequence (mean-field model to 3D-Heisenberg to 3D-XY to 3D-Ising) can be overruled if the temperature region in which the 3D-Heisenberg model could suitably describe the system is overlapped by the region in which the magnetic anisotropies are important. They were able to evaluate in that case the crossover temperatures and indeed found an overlap, which did not allow them to see a 3D-Heisenberg behavior but directly a 3D-Ising one, as it is now the case with $Pr_{0.6}Sr_{0.4}MnO_3$ and $Nd_{0.6}Sr_{0.4}MnO_3$.

As stated in the Introduction, the critical behavior of $Pr_{0.6}Sr_{0.4}MnO_3$ has already been studied by Hcini *et al.* [20], Rößler *et al.* [21], and Masheswar Repaka *et al.* [22], Table III

presents the critical exponents found in those studies together with the ones obtained in the present paper; all the rest of the critical exponents cited in the Introduction have also been included in that table. In order to compare the quality of the results, some things must be considered, apart from the final figures given in each paper: the type of crystals, the particular experiments performed, and the data treatment; the way parallelism is checked or arrived at for the MAPs; and the number of points used for the fit in the Kouvel Fisher method are hints of the rigor employed in extracting conclusions from the data. Though δ is not a good discriminator among models (as it is too similar for several of them), the critical isotherm method from which it is extracted is important to verify if indeed theory is complied in a wide enough region of magnetic field and to check the fulfillment of Eq. (7) so that everything is coherent. Finally, the fulfillment of the magnetic equation of state [Eq. (5)] with the curves collapsing in two independent branches is also a strong indicator of the quality of the study. So all of this must be taken into account besides the particular values of α,β,γ in Table III. It has already been pointed out in the Introduction that the specific heat critical parameters are the most reliable because of the bigger difference among models.

In the three cases mentioned above for $Pr_{0.6}Sr_{0.4}MnO_3$, the conclusions were that this particular composition belongs to the Heisenberg class. But in the first and the third papers, the samples were not single crystals. The transitions are heavily rounded in the near vicinity of the critical temperature in polycrystals compared to single crystals, making it more difficult to reveal the possible nonisotropic features in the critical behavior, as the critical exponents are extracted from the shape of the transition close enough to T_C. Thus, average effects can arise in polycrystals. Besides, in Ref. [20], the parallelism of the MAP curves for the Heisenberg case is nearly nonexistent, the number of points for the Kouvel Fisher plots is too small to draw significant conclusions, and the value for $\gamma(1.304)$ is really in the middle of the ones for Heisenberg and Ising (1.386–1.237). Reference [22] only presents the MAP, there is no further analysis (Kouvel Fisher, critical isotherm, magnetic equation of state, etc.). Reference [21], on the other hand, is a very complete study done using single crystals. Though their conclusion is that the Heisenberg model is of application, they also ascertain that their MAPs give straight parallel lines both for the Heisenberg and Ising theoretical values (though they only show the first one so it is not possible to make the comparison). In several occasions through the paper, they affirm that there is an expected crossover to a 3D-Ising model but that they are not able to see it. Finally, the information about the critical exponent α is extracted from a specific heat curve with low resolution; higher resolution measurements are necessary to be able to discriminate among the different short range models (they do not mention whether a fitting with the Ising values was tried, for instance). In their conclusions they accept that the magnetic anisotropy influences the scaling analysis even if they do not obtain the Ising exponents, as it has happened with our paper.

Concerning $Nd_{0.6}Sr_{0.4}MnO_3$, its critical behavior has only been studied once, to our knowledge, using the inverse of thermal diffusivity, and the conclusion was that it corresponded to the Ising universality class [25]. This last study was done with a single crystal different to the one used here, grown at another lab. The only close composition studied (which corresponds to a similar phase diagram) is $Nd_{0.7}Sr_{0.3}MnO_3$, and the conclusion was that the critical exponents were in-between the mean field model and the Heisenberg case, but, unfortunately, the quality of the MAP, Kouvel Fisher, and scaling plots is not as good as in this case [24].

What is not yet clear is the origin of the magnetocrystalline anisotropies that make $Pr_{0.6}Sr_{0.4}MnO_3$ and $Nd_{0.6}Sr_{0.4}MnO_3$ well described by the 3D-Ising universality class. A first possibility is the rare-earth magnetism of Pr and Nd, which might interact with the manganese spin network, as it has been proposed in some manganites [21,34]. Besides, it must be taken into account that although these concentrations ($x = 0.4$) are thought to be far from the charge-ordered antiferromagnetic phase with charge localization ($x = 0.5$) where phase segregation is well established [35], in some studies it was found that $Nd_{1-x}Sr_xMnO_3$ ($x = 0.3,0.4$) also presented a weaker mechanism of carrier localization as well as phase segregation [36–38]. In other papers for $x = 0.3$, a competition between the double exchange mechanism and correlations arising from coupled spin and lattices degrees of freedom was found [24,37]. All of this suggests that the paramagnetic to ferromagnetic transition at these concentrations is not a conventional continuous phase transition. In fact, the CMR effects observed in manganites have been theorized to be related to the formation of correlated magnetic polarons as well as electronic phase separation [39]. The way this might affect the description of the critical behavior is still a question to be developed from the theoretical point of view. Bear in mind that if a ferromagnetic system is simply and fully described by the double-exchange mechanism, theory assesses that it should be described by the 3D-Heisenberg model [8]. This implies that the description of these ferromagnetic transitions is much more complex than thought.

So far, we have only included in the comparisons the manganite systems that are very similar (from the point of view of the phase diagram) to the concentrations studied in this paper, but the comparison can also be made with a broader perspective to include other manganite systems whose critical behavior has been studied as well. Table III contains all the critical parameters in the papers cited in what follows. After Dagotto *et al.*'s classification, the manganites systems can be subdivided into large-bandwidth manganites (as $La_{1-x}Sr_xMnO_3$), intermediate-bandwidth manganites (as $La_{1-x}Ca_xMnO_3$), and low-bandwidth manganites (as $Pr_{1-x}Ca_xMnO_3$), with phase diagrams very different from one group to another, though there are certain similarities at particular concentrations [40]. Though $Nd_{1-x}Sr_xMnO_3$ could be included in the intermediate-bandwidth group due to the presence of a charge-order phase in a thin range of concentrations, the general aspect of the phase diagram is much more similar to that of $La_{1-x}Sr_xMnO_3$. The $Pr_{1-x}Sr_xMnO_3$ phase diagram is certainly closer to $La_{1-x}Sr_xMnO_3$ than to $Pr_{1-x}Ca_xMnO_3$, which does not even have a ferromagnetic metallic phase but an insulator one. This means that $Nd_{1-x}Sr_xMnO_3$ and $Pr_{1-x}Sr_xMnO_3$ fall better in the large-bandwidth group. The critical behavior of $La_{1-x}Ca_xMnO_3$ and $Pr_{1-x}Ca_xMnO_3$ has also been studied lately at the same time that their phase diagrams have been

refined. $La_{0.6}Ca_{0.4}MnO_3$ is not a good comparison with the samples studied in this paper, as there is a tricritical point at that concentration, with critical exponents obtained in agreement with that tricriticality [41,42]. An interesting result is that in $La_{1-x}Ca_xMnO_3$ the 3D-Heisenberg model is only of application for $x < 0.2$, having observed severe deviations at $x \geqslant 0.2$ (at $x = 0.3$ there is even a first order transition) [43,44]. In particular, at $x = 0.2$, the observed critical exponents are between the 3D-Heisenberg and the 3D-Ising model [42]. On the other hand, $Pr_{1-x}Ca_xMnO_3$ has been found to agree with the Heisenberg model for $x = 0.25, 0.27$, but there are discrepancies for $x = 0.3$ where a mean-field model behavior has also been found [27,45]. The general conclusion from this broad comparison is that critical behavior is especially complex when hole- or electron-doping is higher than a certain minimum value and that the evolution of the critical exponents with doping is different in the three big families. Our paper as well as other literature results suggest that the 3D-Ising behavior needs to be strongly taken into account in the large-bandwidth manganites at intermediate concentrations, as plainly seen in Table III.

Finally, we can go further and compare the critical behavior found in this paper with the one observed for $R_{1-x}Sr_xMnO_3$ ($R = Pr, Nd$), with x close to 0.5 (where charge order and charge localization are well established): they have in common that anisotropies also need to be taken into account to explain the experimental results. The critical exponents found in those cases are between the mean field model and the 3D-Heisenberg class, and a new universality class has been proposed where the Hamiltonian could combine a model of two-dimensional Heisenberg spins with long range interaction [46,47]. A magnetostructural coupling has been found for the case of $R = Pr$ [35], while for $R = Nd$ long-range dipolar interactions have been invoked to explain the deviations from the exchange regime [48].

This implies that much more experimental work is needed to fully characterize the magnetism of $R_{1-x}Sr_xMnO_3$ ($R = Pr, Nd$) with $x = 0.4$. Besides, it would also be interesting to perform complete critical behavior studies in more manganites $R_{1-x}Sr_xMnO_3$ ($0.25 \leqslant x \leqslant 0.45$), extracting independently α, β, γ, and δ, to fully evaluate the extension of the universality of the Ising class in this range, as several studies point out through the years.

V. CONCLUSIONS

A comprehensive and detailed critical behavior study of the paramagnetic to ferromagnetic transition in $R_{0.6}Sr_{0.4}MnO_3$ manganites ($R = Pr, Nd$) has been carried out using magnetic as well as calorimetric techniques in order to independently extract the critical exponents α, β, γ, and δ. In each case ($R =$ Pr or Nd), the values of these exponents match among them and correspond to the 3D-Ising universality class, indicating that the description of the magnetic transition must take into account the existence of mechanisms that introduce magnetocrystalline anisotropies in the system and thus cannot be simply described by the expected double exchange mechanism. Further studies concerning the magnetism of these systems should be undertaken in order to find a theoretical explanation for this anisotropy.

ACKNOWLEDGMENTS

This work have been supported by Ministerio de Ciencia e Innovación with FEDER support (grant MAT2011-23811), Gobierno Vasco (grant IT619-13), and UPV/EHU (grant UFI11/55). Work at the University of Warwick was supported by EPSRC, UK (grant EP/I007210/1). The authors thank for technical and human support provided by SGIker of UPV/EHU.

[1] H. E. Stanley, *Introduction to Phase Transitions and Critical Phenomena* (Oxford University Press, Oxford, 1971).
[2] R. Guida and J. Zinn-Justin, J. Phys. A: Math Gen. **31**, 8103 (1998).
[3] M. Campostrini, M. Hasenbusch, A. Pelissetto, P. Rossi, and E. Vicari, Phys. Rev. B **63**, 214503 (2001).
[4] M. Campostrini, M. Hasenbusch, A. Pelissetto, P. Rossi, and E. Vicari, Phys. Rev. B **65**, 144520 (2002).
[5] M. Hasenbusch, Phys. Rev. B **82**, 174434 (2010).
[6] H. Kuwahara, R. Kawasaki, Y. Hirobe, S. Kodama, and A. Kakishima, J. Appl. Phys. **93**, 7367 (2003).
[7] C. Martin, A. Maignan, M. Hervieu, and B. Raveau, Phys. Rev. B **60**, 12191 (1999).
[8] N. Furukawa and Y. Motome, Appl. Phys. A **74**, S1728 (2002).
[9] A. Oleaga, A. Salazar, D. Prabhakaran, and A. T. Boothroyd, J. Phys.: Condens. Matter **17**, 6729 (2005).
[10] C. V. Mohan, M. Seeger, H. Kronmüller, P. Murugaraj, and J. Maier, J. Magn. and Magn. Mat. **183**, 348 (1998).
[11] A. Schwartz, M. Scheffler, and S. M. Anlage, Phys. Rev. B **61**, R870 (2000).
[12] S. E. Lofland, V. Ray, P. H. Kim, S. M. Bhagat, M. A. Manheimer, and S. D. Tyagi, Phys. Rev. B **55**, 2749 (1997).
[13] S. Nair, A. Banerjee, A. V. Narlikar, D. Prabhakaran, and A. T. Boothroyd, Phys. Rev. B **68**, 132404 (2003).
[14] K. Ghosh, C. J. Lobb, R. L. Greene, S. G. Karabashev, D. A. Shulyatev, A. A. Arsenov, and Y. Mukovskii, Phys. Rev. Lett. **81**, 4740 (1998).
[15] L. Vasiliu-Doloc and J. W. Lynn, J. Appl. Phys. **83**, 7342 (1998).
[16] M. C. Martin, G. Shirane, Y. Endoh, K. Hirota, Y. Moritomo, and Y. Tokura, Phys. Rev. B **53**, 14285 (1996).
[17] D. Kim, B. L. Zink, F. Hellman, and J. M. D. Coey, Phys. Rev. B **65**, 214424 (2002).
[18] A. Oleaga, A. Salazar, D. Prabhakaran, and A. T. Boothroyd, Phys. Rev. B **70**, 184402 (2004).
[19] P. Lin, S. H. Chun, M. B. Salamon, Y. Tomioka, and Y. Tokura, J. Appl. Phys. **87**, 5825 (2000).
[20] S. Hcini, S. Zemni, M. Baazaoui, J. Dhahri, H. Vincent, and M. Oumezzine, Solid State Sciences **14**, 644 (2012).
[21] S. Rößler, H. S. Nair, U. K. Rößler, C. M. N. Kumar, S. Elizabeth, and S. Wirth, Phys. Rev. B **84**, 184422 (2011).

[22] D. V. Masheswar Repaka, T. S. Tripathi, M. Aparnadevi, and R. Mahendiran, J. Appl. Phys. **112**, 123915 (2012).
[23] J. Fan, L. Pi, L. Zhang, W. Tong, L. Ling, B. Hong, Y. Shi, W. Zhang, D. Lu, and Y. Zhang, Appl. Phys. Lett. **98**, 1072508 (2011).
[24] R. Venkatesh, M. Pattabiraman, S. Angappane, G. Rangarajan, K. Sethupathi, J. Karatha, M. Fecioru-Morariu, R. M. Ghadimi, and G. Guntherodt, Phys. Rev. B **75**, 224415 (2007).
[25] A. Oleaga, A. Salazar, and K. Kuwahara, Physica B **378–380**, 512 (2006).
[26] A. J. Campbell, G. Balakrishnan, M. R. Lees, D. McK. Paul, and G. J. McIntyre, Phys. Rev. B **55**, R8622 (1997).
[27] W. Jiang, X. Z. Zhou, G. Williams, Y. Mukovskii, and K. Glazyrin, Phys. Rev. B **78**, 144409 (2008).
[28] A. Oleaga, A. Salazar, and Yu. M. Bunkov, J. Phys.: Condens. Matter **26**, 096001 (2014).
[29] M. Marinelli, U. Zammit, F. Mercuri, and R. Pizzoferrato, J. Appl. Phys. **72**, 1096 (1992).
[30] A. Salazar, Rev. Sci. Instrum. **74**, 825 (2003).
[31] S. K. Banerjee, Phys. Lett. **12**, 16 (1964).
[32] J. S. Kouvel and M. E. Fisher, Phys. Rev. **136**, A1626 (1964).
[33] U. Zammit, M. Marinelli, F. Mercuri, S. Paoloni, and F. Scudieri, Rev. Scient. Inst. **82**, 121101 (2011).
[34] A. Oleaga, A. Salazar, D. Prabhakaran, J. G. Cheng, and J. S. Zhou, Phys. Rev. B **85**, 184425 (2012).
[35] A. K. Pramanik, R. Ranjaan, and A. Banerjee, J. Magn. Magn. Mater. **325**, 29 (2013).
[36] M. Pattabiraman, P. Murugaraj, G. Rangarajan, C. Dimitropoulos, J. Ph. Ansermet, G. Papavassiliou, G. Balakrishnan, D. McK. Paul, and M. R. Lees, Phys. Rev. B **66**, 224415 (2002).
[37] T. Y. Koo, V. Kiryuikhin, P. A. Sharma, J. P. Hill, and S.-W. Cheong, Phys. Rev. B **64**, 220405(R) (2001).
[38] K. Y. Choi, P. Lemmens, G. Güntherodt, M. Pattabiraman, G. Rangarajan, V. P. Gnezdilov, G. Balakrishnan, D. McK. Paul, and M. R. Lees, J. Phys.: Condens. Matter **15**, 3333 (2003).
[39] Y. Tokura, Rep. Prog. Phys. **69**, 797 (2006).
[40] E. Dagotto, T. Hotta, and A. Moreo, Phys. Reports **344**, 1 (2001).
[41] D. Kim, B. Revaz, B. L. Zink, F. Hellman, J. J. Rhyne, and J. F. Mitchell, Phys. Rev. Lett. **89**, 227202 (2002).
[42] P. Zhang, P. Lampen, T. L. Phan, S. C. Yu, T. D. Thanh, N. H. Dan, V. D. Lam, H. Srikanth, and M. H. Phan, J. Magn. Magn. Mater. **348**, 146 (2013).
[43] W. Jiang, X. Zhou, G. Williams, Y. Mukovskii, and R. Privenzentsev, J. Phys.: Condens. Matter **21**, 415603 (2009).
[44] P. M. G. L. Ferreira and J. A. Souza, J. Phys.: Condens. Matter **23**, 226003 (2011).
[45] T. A. Ho, T. D. Thanh, Y. Yu, D. M. Tartarovsky, T. O. Ho, P. D. Thang, A.-T. Lee, T.-L. Phan, and S. C. Yu, J. Appl. Phys. **117**, 17D122 (2015).
[46] A. K. Pramanik and A. Banerjee, Phys. Rev. B **79**, 214426 (2009).
[47] Sk. Sabyasachi, A. Bhattacharayya, S. Majumdar, S. Giri, and T. Chatterji, J. Alloys Comp. **577**, 165 (2013).
[48] V. V. Krishnamurthy, I. Watanabe, K. Nagamine, H. Kuwahara, and Y. Tokura, Phys. Rev. B **61**, 4060 (2000).